

# Potential of Mean Force of Ion Permeation through $\alpha 7$ nAChR Ion Channel

Jens Krüger and Gregor Fels\*

Department of Chemistry, University of Paderborn, Warburger Strasse 100, 33100 Paderborn, Germany  
fels@uni-paderborn.de

Associate Editor: Sandra Gesing and Jano van Hemert

---

## ABSTRACT

Many neuronal diseases such as Alzheimer's dementia are related to a loss of inter-neuron communication. The nicotinic acetylcholine receptor (nAChR) plays a crucial role in this process and is severely affected upon disease progression. Successful therapy approaches rely on modulation of response signals, initiated by the flux of ions through the receptor integrated ion channel at the post-synaptic membrane. We here present the comparison of two methods for calculating the potential of mean force of nAChR mediated ion permeation, in terms of accuracy and performance.

## 1 INTRODUCTION

The nicotinic acetylcholine receptor (nAChR) is a cation-selective channel made up from five homologous subunits symmetrically arranged around a central pore, thus forming a structure with five-fold pseudo-symmetry (Lester et al. 2004). The nAChR at the neuromuscular endplate is a heteropentamer with  $\alpha_2\beta\gamma\delta$  subunits, while the neuronal receptor type used in this study is an  $\alpha 7$  homopentamer. Cryo-electron microscopy studies of the *Torpedo marmorata* nAChR have revealed three domains: an extracellular domain hosting the neurotransmitter binding sites; a transmembrane domain forming a channel across the cell wall and an intracellular domain providing binding sites for cytoskeletal proteins (Miyazawa et al. 2003; Unwin 2005). The extracellular part of the protein is homologous to that of the acetylcholine binding protein found in the snail *Lymnaea stagnalis* (Brejc et al. 2001). The transmembrane domains of each subunit consist of four membrane spanning helices named M1 to M4. The M2 helix is the pore lining part while M4 faces the lipid environment.

The nAChR plays a crucial role in neuronal signaling and therefore holds a key function for learning and memory processes. It is severely affected by neuronal diseases such as Alzheimer's dementia (Gotti and Clementi 2004). When an action potential arrives at the presynaptic membrane of a neuronal synapse, a biochemical cascade leads to the release of the neurotransmitter acetylcholine. Upon binding of two acetylcholine molecules to the extracellular part of nAChR at the postsynaptic membrane, the integrated ion channel, located over 20 Å away from the ligand binding site, is

opened, enabling the influx of  $\text{Na}^+$  and  $\text{Ca}^{2+}$  ions and the efflux of  $\text{K}^+$  ions (Fels et al. 1982). This causes a change in electrical potential on the postsynaptic membrane that in turn enables the further propagation of the neuronal action potential (Buckingham et al. 2009). Individuals affected by Alzheimer's dementia lack a sufficient number of functional postsynaptic nAChR. Hence, the influx of  $\text{Na}^+$  is not sufficient to depolarize the membrane and to ignite a new action potential (Buckingham et al. 2009). Accordingly, understanding the gating mechanism of nAChR ion channels should be helpful in improving symptomatic Alzheimer's therapy.

We have evaluated and compared two methods for the calculation of the potential of mean force (PMF) of ion permeation through the nAChR, Umbrella Sampling (US) and Steered Molecular Dynamics (SMD) pulling, in order to understand the changes in electrical potentials connected to channel gating. The PMF corresponds to the barrier a permeating ion has to overcome. It is crucial for the understanding of selectivity and conductivity of the nAChR. The required simulation steps as well as the quality of the resulting PMFs have been evaluated and are presented in a comparative manner. Special emphasis lies in the performance on two different high performance computing clusters (HPC) and the influence on required CPU hours and real simulation time.

## 2 METHODS

A homology model for the transmembrane part of human  $\alpha 7$  nAChR was constructed on the basis of an electron microscopy structure of *torpedo marmorata* (PDB code 1OED) (Unwin 2005). The details of homology modeling are described elsewhere (Kelly 1999; Wallace and Roberts 2004; Gomaa et al. 2007). In brief, after aligning the sequence (SwissProt code P36544) (Peng et al. 1994) with the template, backbone positions are assigned for identical residues. Then loops are generated and candidates are chosen according to a Boltzman-weighted criterion. Then side chain data is assembled from an extensive rotamer library. The best intermediate model is chosen based on electrostatic solvation energy and/or a packing score and finalized by energy minimization. The procedure is included in MOE-2008.10. (Molecular Operating Environment Chemical Computing Group, Inc., 1010 Sherbrooke St. W, Suite 910 Montreal, Quebec, Canada H3A 2R7)

All MD simulation were carried out using GROMACS-4.0.4 (van der Spoel et al. 2005; Hess et al. 2008) with the Gromos96 (ffG45a3) force field (Schuler et al. 2001). The temperature of the peptide, lipid and the solvent were separately coupled to a  $v$ -rescale thermostat with a coupling time of

---

\*To whom correspondence should be addressed.

0.1 ps. Semi-isotropic pressure coupling was applied with a coupling time of 1.0 ps and a compressibility of  $4.5 \cdot 10^{-5} \text{ bar}^{-1}$  for the xy-plane as well as for the z-direction. Long range electrostatics were calculated using the particle-mesh Ewald (PME) algorithm with grid dimensions of 0.12 nm and interpolation order 4. Lennard-Jones and short-range Coulomb interactions were cut off at 1.4 and 0.8 nm respectively.

The topology for the lipid bilayer (POPC (16:0-18:1 Diester PC, 1-Palmitoyl-2-Oleoyl-*sn*-Glycero-3-Phosphocholine) are the same used in earlier studies (Krüger and Fischer 2008) and were originally created on the basis of the parameters of Chandrasekhar et al. (Chandrasekhar et al. 2003).

Each pore model was embedded into a hydrated POPC bilayer system, by removing overlapping lipid and water molecules. After minimization the systems were equilibrated for 3x1 ns while initial position constraints were stepwise reduced (protein, backbone, C-alpha). In order to reduce stress induced by lateral pressure fluctuations each pore model was simulated during the equilibration phase using surface-tension pressure coupling with a tension of 37.5 mN/m (Krüger and Fischer 2009). The complete systems for US and pulling SMD consisted of the protein, 250 POPC, 17250 SPC-waters, 537  $\text{Na}^+$  and 512  $\text{Cl}^-$ .

US simulations follow the procedure described by Hub and de Groot (Hub and de Groot 2008). Only pressure coupling in the xy-plane was enabled while keeping the z-direction fixed. The starting configurations for the US simulations are based on three 10 ns equilibrium simulations. Three distinct channel conformations were prepared as described above and a full set of US simulations carried out for each of them. The channels were divided into 0.25 Å wide sections along the central pore axis. The ion was placed subsequently into the center of each section, removing overlapping waters, followed by a thorough energy minimization. A harmonic restraint of 4000 kJ/mol was applied on the ion position along the pore axis. The subsequent simulations were carried out for 300 ps each.

The PMFs were constructed with the WHAM procedure of Hub and de Groot (Hub and de Groot 2008) implemented into *g\_wham* included in GROMCAS. The first 50 ps were omitted and a cyclic correction for the periodic system was applied, using an alpha of 1.75. The statistical error was estimated with a bootstrap analysis ( $N = 42$ ).

During pulling SMD semi-isotropic pressure coupling was used applying 1 bar in z-direction while keeping the xy-plane fixed. The ion was placed at the top or bottom of the simulation system on the central pore axis. The virtual spring attached to the ion had a constant of 100 kJ/mol/nm<sup>2</sup> and was moved at 0.00375 nm/ns. Two times twelve independent simulations were carried out, pulling the ion through the pore from either side.

The construction of PMFs follows the method of Anishkin and Sukharev (Anishkin and Sukharev 2004) considering the pulling as irreversible work against the opposing friction forces and assuming a constant friction coefficient. The friction coefficient was fitted for each independent simulation till both ends equal a zero potential, which reflects the boundary condition of a free ion in bulk water.

The error estimate for the SMD PMFs was calculated using block averaging considering them to be correlated fluctuating quantity. The sets are divided in a number of blocks and averages are calculated for each block. The error for the total average is calculated from the variance between averages of the  $m$  blocks  $\mathcal{B}_i$  as follows:  $\text{stderr}^2 = \sum (\mathcal{B}_i - \langle \mathcal{B} \rangle)^2 / (m(m-1))$ . The complete derivation is given in the literature (Hess 2002).

The simulations were run on a DELL Studio XPS (8 cores, i7 920) and on facilities of the Paderborn Center for Parallel Computing PC<sup>2</sup> (<http://www.wcs.uni-paderborn.de/pc2/>, Arminius (400 cores, Xeon 3.2 GHz EM64T, Infiniband) and Bisgrid (64 cores, dual-core Opteron 2.8 GHz, Infiniband)).

Plots and pictures were made with Xmgrace-5.1.22, VMD-1.8.7 and MOE-2008.10.

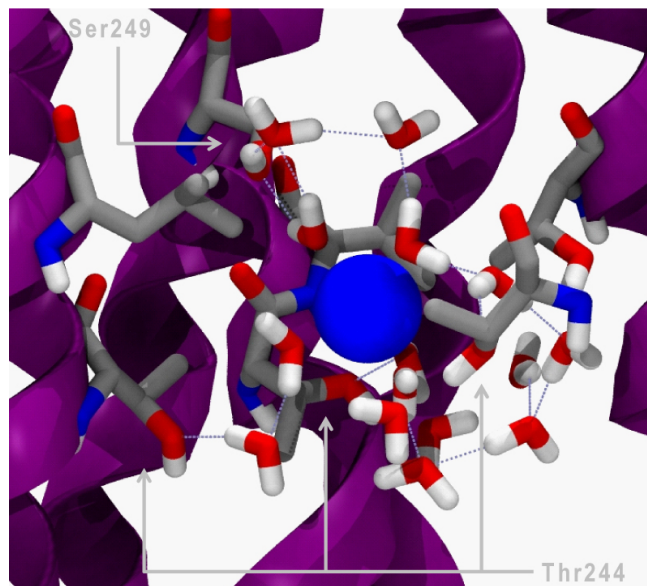


**Fig. 1.** Close view on the sodium ion at the gorge portion of the pore. While the hydration shell is slightly deformed in this confined space Thr244 and Ser249 show a stabilizing interaction. The hydrogen bond network is shown by dotted blue lines.

### 3 RESULTS

The sodium ion permeation through the nAChR was studied with two different methods for the construction of PMFs. The PMFs represent the energy barrier a passing ion has to overcome. This barrier is directly correlated to conductivities accessible by experiments. Therefore PMFs are invaluable tools to access scientific problems such as ion selectivity, channel open-/closing, mutations inside the pore or allosteric modulation.

Basically a PMF describes the probability to encounter the ion at a certain position along the reaction coordinate, compared to the bulk phase (equation 1).

$$PMF(z) = -k_B T \ln(P(z)/P_0) \quad (1)$$

For US, which can be applied to a broad variety of other problems, the probability is derived from umbrella histograms of the restrained atom (Kumar et al. 1992; Kumar et al. 1995; Beckstein and Sansom 2006; Hub and de Groot 2008).

The construction of PMFs for pulling SMD follows the Langevin equation (equation 2) considering the forces exerted on the ion along the reaction coordinate as irreversible work against the friction force (Gullingsrud et al. 1999; Anishkin and Sukharev 2004).

$$PMF(z) = \sum_{n=1}^{N_z} (\langle \Delta F_n \rangle - \gamma \langle \Delta z_n \rangle / \Delta t_n) \Delta z_n \quad (2)$$

Both approaches usually assume that the end points lie within the bulk phase of the solvent. As the ion does not experience any potential at these points, they have to be equal and zero (equation 3).

$$PMF(z_{start}) = PMF(z_{end}) = 0 \quad (3)$$

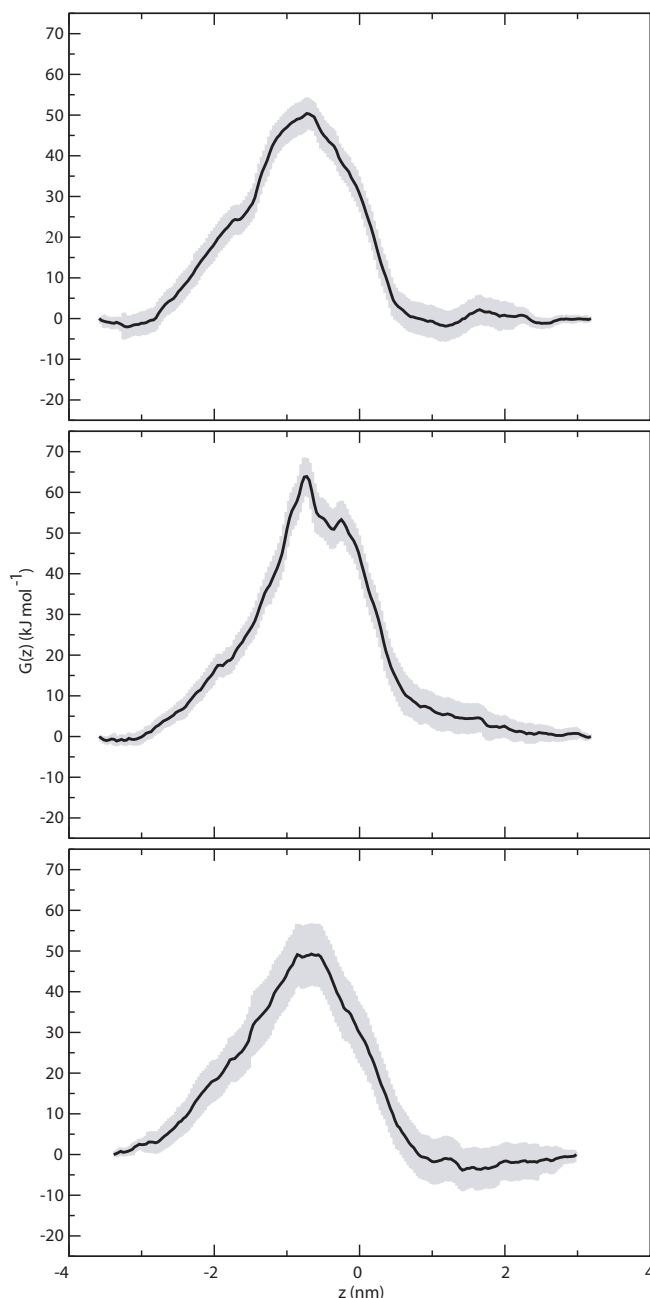


**Fig. 2.** PMF for the permeation of  $\text{Na}^+$  through the nAChR derived by US. The three curves are based on the same structural model, but each starting configuration was prepared in a slightly different way. The permeation barrier lies for all three independent simulations between 50 and 60 kJ/mol. The gray areas correspond to the standard deviation derived by bootstrap analysis.

The conductive properties and time dependent characteristics of an ion channel are determined by various features of the pore, as well as the influence of the extra- and intra-cellular parts. Beside general aspects like the length of the pore and its diameter, the orientation and polarity of side chains pointing into the lumen of the pore are highly relevant. The energy barrier of ion permeation not only has an enthalpic part but usually has also a large entropic part (Portella et al. 2008). As the hydrated ion enters the mouth of the pore the move ability of waters between the protein and the ion is more limited. Consequently degrees of freedom are lost such as rotational and translational degrees for the waters as well as the protein side chains. The ion experiences repulsion and stabilization depending on the specific topology of the channel. Hydrophobicity and hydrophilicity determine how well a passing ion is stabilized within the narrow part of the pore (Krüger and Fischer 2009). It can be stated that first hydration shell of the sodium ion inside the nAChR pore is never removed. At the gorge portion of the pore deformations can be observed (Figure 1), which are directly stabilized by serine and threonine residues (Thr244 and Ser249), which are found in rings along the pore (Bertrand et al. 1993). The sophisticated counter play between hydrophilic (e.g. Ser and Thr) and hydrophobic (e.g. Leu and Ile) residues in the gorge area of the channel determines its conductivity and selectivity.

### 3.1 Umbrella Sampling

US simulations yield robust and well reproducible PMFs as long as a high sampling density can be achieved. This can be a challenging endeavor if the probability to encounter the ion at the gorge portion of a pore is low. Related to this problem is the artificial (partial) loss of the hydration shell of the ion during system preparation, when it is placed in hydrophobic areas of the pore.

Another commonly observed effect for pore US is due to small sampling errors, that the ends of the PMF are not equal unlike being proposed in equation 3. This effect can be overcome with cyclic correction as described by Hub and de Groot (Hub and de Groot 2008).

In this study the nAChR channel was prepared in three slightly different ways, yielding three identical systems in terms of sequence, secondary structure, lipid environment and solvent content. The difference lies within the small conformational diversity. For each of them at least 300 restrained US were carried out. The single 300 ps simulations took 7.8 hours each using 4 cores.

The height of the PMFs was determined to be 51.4, 63.1 and 49.5 kJ/mol. The standard deviation for US PMFs determined by bootstrap analysis is in most cases around 2.5 kJ/mol, but in some cases can reach as high as 7.6 kJ/mol (Figure 2). This is largely influenced by the convergence of each simulation. Especially for the gorge portion of the channel larger deviations have to be expected.

An earlier study using US on restrained nAChR-M2 helices embedded into a bilayer-mimetic slab made from CH<sub>4</sub> molecules reports a barrier of 10.5  $k_B T$  for the sodium ion permeation (Beckstein and Sansom 2006). These are just 25.5 kJ/mol or factor 2 less than the results presented in this study. The deviation has to be contributed to the simulation conditions or more likely to the analysis. The block data created by the modified WHAM analysis tool from Alan Grossfield (<http://membrane.urmc.rochester.edu/wham>) used in that study can easily be misrepresented in Xmgrace by a factor of 2. The misinterpretation has to be presumed comparing to

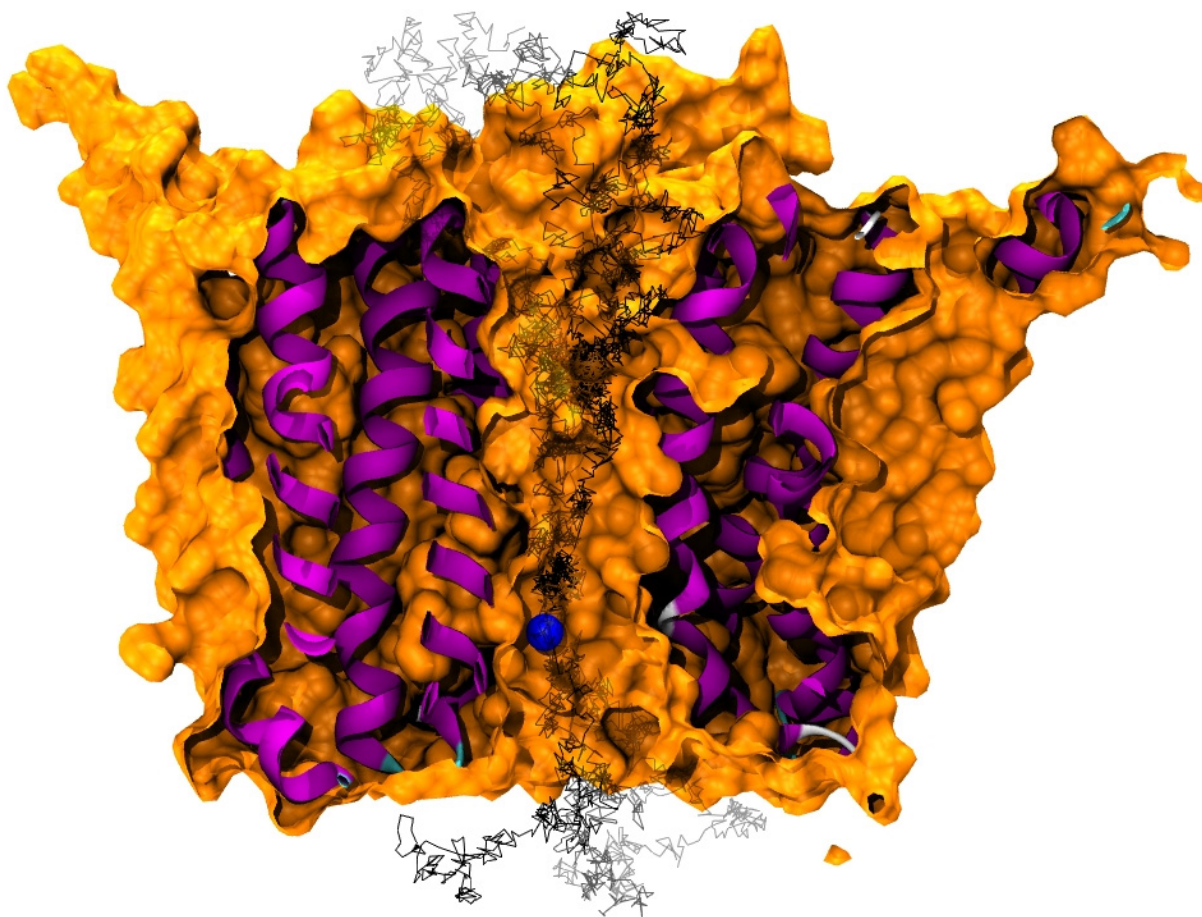


**Fig. 3.** Cut through the transmembrane part of the nAChR (orange, purple helices). Three independent permeation pathways of  $\text{Na}^+$  (blue) are indicated by thin gray lines, which are derived from different SMD pullings.

the PMF heights determined in this study using two different methods.

### 3.2 Steered Molecular Dynamics - Pulling

When an ion is pulled through a pore like the transmembrane part of the nAChR it follows the natural path the ion would take in a living organism. As shown in Figure 3 this path may vary significantly for each individual permeation event. Hence different distances were covered in different times, yielding slightly different velocities. Therefore the friction coefficient has to be recalculated for each simulation separately in order to fulfill equation 3.

The shape of pulling PMFs is slightly deformed as a constant friction coefficient was used. It was suggested by Gullingsrud et. al. to use a velocity autocorrelation approach in order to apply a modulated friction coefficient along the reaction coordinate (Gullingsrud et al. 1999). As Patargias et. al. have demonstrated on restraint Vpu pores, this approach negates the deformation (Patargias et al. 2009). Unfortunately the ion experiences a complete different microenvironment at the mouth of the pore than it does within the gorge portion. Therefore the autocorrelation approach used in that study easily overestimates the friction within the pore yielding a too low potential. For this study it was found to be more acceptable to have an unphysical deformation with accurate error

estimate than having an unphysical flattening of the potential with uncertain error. Ongoing research aims at overcoming this problem. In terms of computational cost the two pulling analysis do not bear any differences.

According to equation 2 different pulling velocities should not affect the final PMF. In order to evaluate the dependence of the friction coefficient on different pulling velocities a sodium ion was pulled through the nAChR pore with 4 different velocities, each with 6 repetitions. As shown in Figure 4 the absolute height of the PMFs is not affected within the margin of error. The increasing minimum around -2 nm has to be contributed to the assumption of a constant friction coefficient. The higher the velocity of the ion the less this assumption holds true. As stated above the deformation of the PMF is related to this limitation. For the highest pulling velocities of 0.03 nm/ns a flattening of the energy barrier can be observed. This effect is best described as ‘rupture’. The ion develops such a high speed that it cannot develop all atomic interactions with surrounding residues. This can be compared to an experimental condition under strong electric field called ‘electroporation’ showing analogy to some extent (Böckmann et al. 2008).

The PMF for pulling from the N- to the C-terminus is shown in the upper panel of Figure 5, while the PMF for the opposite direction is shown below. Mimicking the influx of sodium into the cell

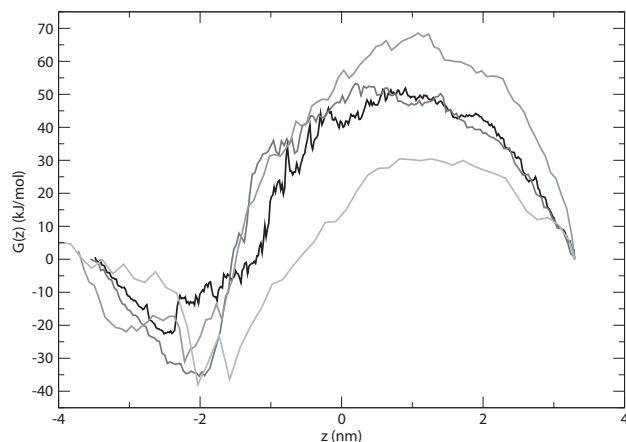


**Fig. 4.** Dependency on pulling velocity. The darkest curve corresponds to a pulling velocity of 0.00375 nm/ns, the velocity of the spring. The speed was doubled with each grayscale. Each individual curve is based on 6 repetitions with a standard error (omitted for clarity) similar to Figure 5. It can be stated that the minimum around -2 nm, which is considered to be an artificial deformation, increases with higher speeds. For the highest speed of 0.03 nm/ns (lightest gray) an effect best described as ‘rupture’ can be observed.

yields a maximum barrier height of  $52.7 \pm 11.1$  kJ/mol, while the efflux has  $57.3 \pm 6.9$  kJ/mol. Assuming that the permeability correlates with  $\exp(-\Delta G_{\max}/k_B T)$  the influx is easier by a factor of 6 (Hub and de Groot 2008). This does not take the estimated error into account which is of the same order of magnitude. This finding is in very good agreement with experimental findings showing that the nAChR is a rather unselective cation channel (Mishina et al. 1986). The evaluation of potassium, calcium and chlorine ion permeation barriers is subject of ongoing research.

The single 2100 ps pulling simulations took 18 hours each using 32 cores. In order to achieve a reasonable error estimate 12 repetitions for the influx and 12 for the efflux were prepared.

### 3.3 Performance

The two methods US and SMD are carried out on identical simulation systems, consisting of exactly the same number of atoms with exactly the same atomic interactions. Although the principals for PMF creation are fundamentally different, in terms of the simulation it is the same to constraint the ion to a certain position along the reaction coordinate or the pull it along the same.

As stated above 300 separate simulations of 300 ps length each are required for the construction of one US PMF. With three repetitions a total of 9360 CPU hours are required. To construct a comparable SMD pulling PMF twelve 2100 ps simulations with 6490 CPU hours are needed. On the first glance the SMD method is one third less expensive than the US method. This conclusion may only be partially true, strongly depending on the architecture of available compute resources. As shown in Figure 6 the simulation setup used in this study scales superlinear on up to 8 cores. Both HPC clusters are equipped with low latency infiniband interconnects, while Arminius has two single-core CPUs (Intel XeonDP 3.2 GHz) on each node, Bisgrid has four dual-core CPUs on each node (AMD Opteron 8220, 2.8 GHz). Although the type of CPU used in both clusters differs by three generations of technological

development the effective performance in ns/day differs only 30 % on 8 cores. The sharing of the same system bus by multiple cores on one node is presumably the main bottle neck hindering better performance on more nodes. This effect is overlaid by the influence of the inter node communication via Infiniband thus leading to the quasi parallel shift observed for large number of cores in Figure 6. Arminius and Bisgrid show a linear speedup on up to 32 and 40 cores, respectively. Using more cores leads to a fall-off of performance. It has to be stated that the simulation system used in this studies was not optimized for highly parallel computing. Aspects like the domain decomposition and grid spacing for PME electrostatics have a considerable impact, especially when using larger numbers of cores (Hess et al. 2008). Additional adjustments would enable further scaling on more cores.

To achieve an optimal investment of computational time a high performance per core was anticipated for US simulating. For SMD it was considered more important to minimize the simulated time (wall clock). The relative short US repetitions (300 ps) can be finished using just 4 cores within 7.8 hours, while the longer SMD simulations (2100 ps) need 18 hours on 32 cores, both measured on Arminius. Considering this discrepancy and comparing to Figure 6 (lower panel) the relative efficiency (ns per day and core) is the highest on 2 cores for both clusters. The level remains high on up

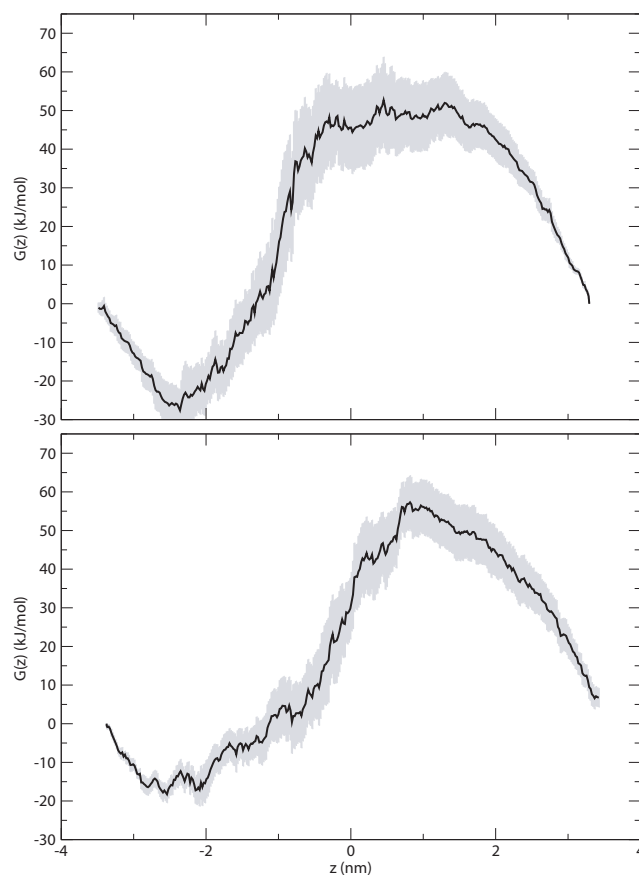


**Fig. 5.** PMFs generated by SMD pulling simulations. The upper panel shows the curve for the  $\text{Na}^+$  influx and the lower panel for the efflux. The barrier height differs by 4.2 kJ/mol or in terms of permeability a factor of 6.

to 8 cores and then drops sharply. The benefits of low latency infiniband interconnects are not used to their full extent. This illustrates clearly that such kind of simulations with GROMACS would be best carried out using distributed computing on multi-core machines.

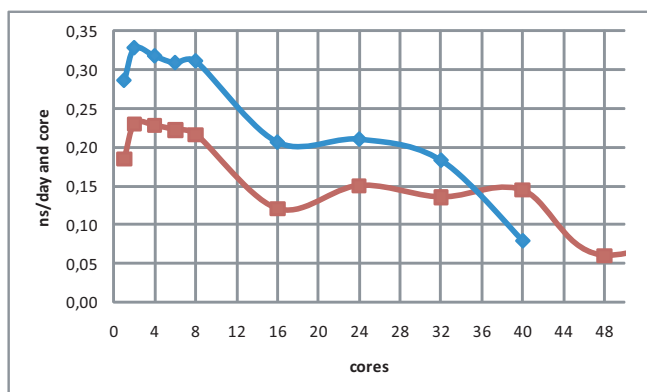
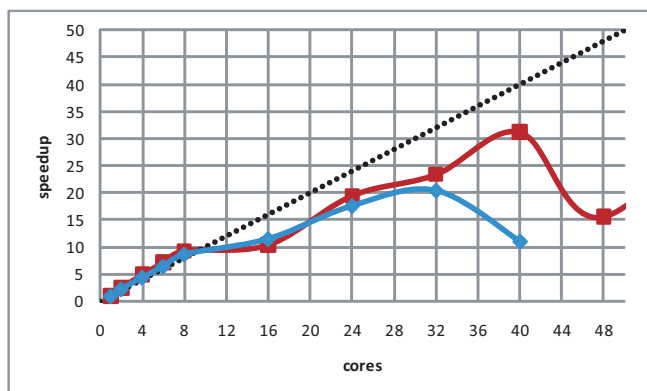
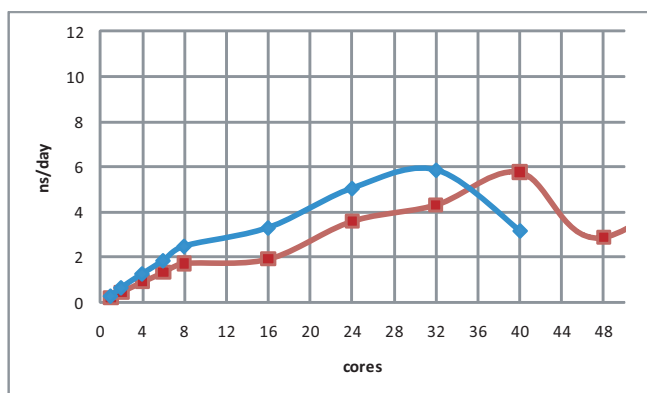


**Fig. 6.** Performance (upper panel), speedup (middle panel) and relative performance (lower panel) of the transmembrane nAChR system presented in this study. The molecular setup consisting of 71994 atoms has been simulated with GROMACS-4.0.4 on two clusters with low latency Infiniband interconnects (blue – Bisgrid: 4 dual-core AMD Opteron 8220, 2.8 GHz per node; red - Arminius: 2 single-core Intel XeonDP, 3.2 GHz per node). On up to 8 cores superlinear scaling could be observed for both systems. Up to 40 cores the speedup increases nearly linear on Arminius, while the performance breaks in at 32 cores on Bisgrid. In order to achieve an optimal investment of computational time a high performance per core was used for US simulating on 4 cores. For SMD it was considered more important to minimize the simulated time (wall clock) and 32 cores were used.

## 4 CONCLUSION

US and SMD based PMFs have been investigated to help understanding cation flux of the nAChR ion channel. Both procedures yield comparable energy barriers for the permeation of  $\text{Na}^+$  through the nAChR. The errors estimated for both methods do not differ considerably. From a technical point of view US tends to be more robust, while SMD enables the differentiation of in- and efflux of ions. Both methods differ by 30 % with respect to the computational cost. Due to the higher number of short simulations required for US this computational procedure is more recommended for low latency distributed computing than SMD.

## ACKNOWLEDGEMENTS

We thank the PC<sup>2</sup> University of Paderborn for providing computer time. JK gratefully acknowledges a research scholarship from the Alexander von Humboldt-Foundation. Support of the e-Science Institute Edinburgh is acknowledged.

## REFERENCES

- Anishkin, A. and S. Sukharev (2004). Water dynamics and dewetting transitions in the small mechanosensitive channel MscS. *Biophys J* **86**(5): 2883-95.
- Beckstein, O. and M. S. Sansom (2006). A hydrophobic gate in an ion channel: the closed state of the nicotinic acetylcholine receptor. *Phys Biol* **3**(2): 147-59.
- Bertrand, D., et al. (1993). Mutations at 2 Distinct Sites within the Channel Domain M2 Alter Calcium Permeability of Neuronal Alpha-7 Nicotinic Receptor. *Proceedings of the National Academy of Sciences of the United States of America* **90**(15): 6971-6975.
- Böckmann, R. A., et al. (2008). Kinetics, statistics, and energetics of lipid membrane electroporation studied by molecular dynamics simulations. *Biophysical Journal* **95**(4): 1837-1850.
- Brejc, K., et al. (2001). Crystal structure of an ACh-binding protein reveals the ligand-binding domain of nicotinic receptors. *Nature* **411**(6835): 269-276.
- Buckingham, S. D., et al. (2009). Nicotinic Acetylcholine Receptor Signalling: Roles in Alzheimer's Disease and Amyloid Neuroprotection. *Pharmacological Reviews* **61**(1): 39-61.
- Chandrasekhar, I., et al. (2003). A consistent potential energy parameter set for lipids: dipalmitoylphosphatidylcholine as a benchmark of the GROMOS96 45A3 force field. *Eur Biophys J* **32**(1): 67-77.
- Fels, G., et al. (1982). Equilibrium Binding of Acetylcholine to the Membrane-Bound Acetylcholine-Receptor. *European Journal of Biochemistry* **127**(1): 31-38.
- Gomaa, M. S., et al. (2007). Homology model of 1 alpha,25-dihydroxyvitamin D-3 24-hydroxylase cytochrome P450 24A1 (CYP24A1): Active site architecture and ligand binding. *Journal of Steroid Biochemistry and Molecular Biology* **104**(1-2): 53-60.
- Gotti, C. and F. Clementi (2004). Neuronal nicotinic receptors: from structure to pathology. *Progress in Neurobiology* **74**(6): 363-396.
- Gullingsrud, J. R., et al. (1999). Reconstructing potentials of mean force through time series analysis of steered molecular dynamics simulations. *Journal of Computational Physics* **151**(1): 190-211.
- Hess, B. (2002). Determining the shear viscosity of model liquids from molecular dynamics simulations. *Journal of Chemical Physics* **116**(1): 209-217.
- Hess, B., et al. (2008). GROMACS 4: Algorithms for highly efficient, load-balanced, and scalable molecular simulation. *Journal of Chemical Theory and Computation* **4**(3): 435-447.
- Hub, J. S. and B. L. de Groot (2008). Mechanism of selectivity in aquaporins and aquaglyceroporins. *Proc Natl Acad Sci U S A* **105**(4): 1198-203.
- Kelly, K. (1999). "3D Bioinformatics and Comparative Protein Modeling in MOE." *Journal of the Chemical Computing Group*, from <http://www.chemcomp.com/journal/bio1999.htm>.

- Krüger, J. and W. B. Fischer (2008). Exploring the conformational space of Vpu from HIV-1: a versatile adaptable protein. *J Comput Chem* **29**(14): 2416-24.
- Krüger, J. and W. B. Fischer (2009). Structural implications of mutations assessed by molecular dynamics: Vpu(1-32) from HIV-1. *Eur Biophys J*.
- Kumar, S., et al. (1992). The Weighted Histogram Analysis Method for Free-Energy Calculations on Biomolecules.1. The Method. *Journal of Computational Chemistry* **13**(8): 1011-1021.
- Kumar, S., et al. (1995). Multidimensional Free-Energy Calculations Using the Weighted Histogram Analysis Method. *Journal of Computational Chemistry* **16**(11): 1339-1350.
- Lester, H. A., et al. (2004). Cys-loop receptors: new twists and turns. *Trends in Neurosciences* **27**(6): 329-336.
- Mishina, M., et al. (1986). Molecular Distinction between Fetal and Adult Forms of Muscle Acetylcholine-Receptor. *Nature* **321**(6068): 406-411.
- Miyazawa, A., et al. (2003). Structure and gating mechanism of the acetylcholine receptor pore. *Nature* **423**(6943): 949-955.
- Patargias, G., et al. (2009). Reconstructing Potentials of Mean Force from Short Steered Molecular Dynamics Simulations of Vpu from HIV-1. *J Biomol Struct Dyn* **27**(1): 1-12.
- Peng, X., et al. (1994). Human Alpha-7-Acetylcholine Receptor - Cloning of the Alpha-7-Subunit from the Sh-Sy5Y Cell-Line and Determination of Pharmacological Properties of Native Receptors and Functional Alpha-7-Homomers Expressed in Xenopus-Oocytes. *Molecular Pharmacology* **45**(3): 546-554.
- Portella, G., et al. (2008). Not only enthalpy: Large entropy contribution to ion permeation barriers in single-file channels. *Biophysical Journal* **95**(5): 2275-2282.
- Schuler, L. D., et al. (2001). Molecular dynamics simulation of n-dodecyl phosphate aggregate structures. *Eur Biophys J* **30**(5): 330-43.
- Unwin, N. (2005). Refined structure of the nicotinic acetylcholine receptor at 4A resolution. *J Mol Biol* **346**(4): 967-89.
- van der Spoel, D., et al. (2005). GROMACS: fast, flexible, and free. *J Comput Chem* **26**(16): 1701-18.
- Wallace, I. S. and D. M. Roberts (2004). Homology modeling of representative sub-families of Arabidopsis major intrinsic proteins. Classification based on the aromatic/arginine selectivity filter. *Plant Physiology* **135**(2): 1059-1068.